Polarization observables in p-d scattering below 30 MeV

A. Kievsky,[1] M. Viviani,[1] and S. Rosati[1,2]
[1]*Istituto Nazionale di Fisica Nucleare, Via Buonarroti 2, I-56100 Pisa, Italy*
[2]*Dipartimento di Fisica, Universita' di Pisa, Via Buonarroti 2, I-56100 Pisa, Italy*
(Received 23 March 2001; published 3 July 2001)

Differential and total breakup cross sections as well as vector and tensor analyzing powers for p-d scattering are studied for energies above the deuteron breakup threshold up to $E_{\rm lab}=28$ MeV. The p-d scattering wave function is expanded in terms of the correlated hyperspherical harmonic basis and the elastic S matrix is obtained using the Kohn variational principle in its complex form. The effects of the Coulomb interaction, which are expected to be important in this energy range, have been rigorously taken into account. The Argonne AV18 interaction and the Urbana URIX three-nucleon potential have been used to perform a comparison to the available experimental data.

DOI: 10.1103/PhysRevC.64.024002 PACS number(s): 25.10.+s, 21.30.−x, 24.70.+s

I. INTRODUCTION

In Ref. [1] the authors recently presented an application of the Kohn variational principle (KVP) in its complex form to calculate the elastic observables in p-d scattering for energies above the deuteron breakup threshold (DBT). The KVP was implemented to describe continuum states of three outgoing particles including the distortion due to the Coulomb interaction in the asymptotic region. Only two energies were considered, $E_{\rm lab}=5$ and 10 MeV. The validity of the KVP for the elastic S matrix describing the $2\rightarrow 2$ process in p-d scattering for energies above the DBT has been extensively discussed in Ref. [2].

In the present paper the analysis of the elastic p-d reaction is extended up to $E_{\rm lab}=28$ MeV, covering the region where Coulomb effects are expected to be important. The large amount of accurate experimental data allows for interesting comparisons. It should be noted that, at present, the analysis of the polarization data at energies above the DBT has been done mainly by comparing n-d calculations to p-d data [3,4]. Differential cross section and vector analyzing power data exist for both n-d and p-d scattering, allowing for an estimate of the Coulomb effects. Conversely, no n-d data are available for the deuteron analyzing powers $iT_{11}, T_{20}, T_{21}, T_{22}$. These quantities are evaluated from experiments using a polarized deuteron beam on unpolarized proton targets. The inverse experiment of unpolarized proton or neutron beams on a polarized deuteron target seems to be extremely difficult at low energies and has not yet been done.

Experiments using charged particles are certainly easier to perform and show smaller error bars than those using a neutral beam. On the other hand, the theoretical description of collisions with more than one charged particle in the final state has represented a difficult problem for many years. In a recent work a complete solution of the reaction $e^-+\mathrm{H}\rightarrow \mathrm{H}^+ + e^- + e^-$ has been obtained by Rescigno *et al.* [5] by transforming the Schrödinger equation using the so-called exterior complex scaling and making use of supercomputers to solve the associated equations numerically. This was the first complete solution of a three-body collision with all the charged particles moving away from each other in the final state. Regarding the p-d reaction, different techniques have been applied so far. The Faddeev equations in momentum space have been adapted to take into account the long-range Coulomb interaction using the screening and renormalization approach [6]. Recently, a detailed comparison between the solutions of the Faddeev equations in configuration space and the KVP has been performed, though restricted to energies below the DBT [7]. In the present work we turn our attention to describing p-d elastic observables above the DBT. In this case the application of the KVP is feasible and the calculation of the elastic S matrix does not require large computational devices.

The study of the three-nucleon ($3N$) continuum provides important information about the capability of modern NN potentials to describe the three-nucleon dynamics. At present, a few realistic NN potentials are available that reproduce a large set of two-nucleon ($2N$) data with $\chi^2\approx 1$ (per datum). They are substantially equivalent in reproducing all the details of the NN scattering, but in the description of nuclear systems with $A>2$ differences appear. In addition, the three-nucleon system is the simplest one in which three-nucleon force (3NF) effects can be studied. The first signal for the necessity of a 3NF comes from the underbinding of the triton when only NN forces are used. Widely used 3NF models are based on the exchange of two pions with an intermediate Δ excitation. In general these models include a certain numbers of parameters which are not precisely determined by theory, so some of them can be taken as free parameters in order to reproduce, for example, the triton or ^{3}He binding energy. As a consequence, other observables which scale with the three-nucleon binding energy improve as well. Examples are the bound state r.m.s radii and the zero energy total cross section in n-d and n-^{3}H scattering. On the contrary, vector and tensor N-d analyzing powers do not present such a scaling.

Accurate measurements of p-d observables below the DBT have been reported recently [8–10]. A comparison of the theoretical predictions to these data shows an underprediction of the deuteron vector analyzing power iT_{11} by $\approx 30\%$ [11]. A similar discrepancy had been observed earlier in the neutron analyzing power A_y, a problem which is usually known as the A_y puzzle [12]. As the energy increases the

observed discrepancies in A_y and iT_{11} reduce and tend to disappear, though not completely, above 30 MeV [3]. Accordingly, the study of these observables over the energy region considered here is important for understanding such a behavior.

Accurate $3N$ and $4N$ scattering wave functions are necessary for calculating a number of nuclear reactions. The technique used in the present work is based on the expansion of the wave function in terms of Jastrow type correlated hyperspherical harmonic (CHH) basis functions. When the correlation factor reduces to a pair correlation function the pair correlated hyperspherical harmonic (PHH) basis is obtained. The CHH and PHH bases have been used to calculate the bound states of the $A=3,4$ nuclei [13,14], N-d scattering [15,16], and p-^{3}He and n-^{3}H scattering [17] at energies below the three-body fragmentation. Moreover, wave functions obtained through those expansions have recently been used to study the radiative capture $p+d\rightarrow {}^3\mathrm{He}+\gamma$ below the DBT [18] and the hep process, namely, the weak capture $p+{}^3\mathrm{He}\rightarrow {}^4\mathrm{He}+e^+ +\nu_e$ at the Gamow peak [19]. These two reactions have considerable astrophysical relevance. The former is the second reaction in the pp solar chain and has a prominent role in the evolution of protostars whereas the hep process plays an important role in the solar neutrino problem. The calculation of the p-d wave functions above the DBT will provide the input for further studies of radiative capture and photodisintegration and electrodisintegration of ^{3}He.

In the present paper we present the results obtained for the differential and total breakup cross sections, nucleon analyzing powers A_y, and deuteron analyzing powers iT_{11}, T_{20}, T_{21}, and T_{22} for N-d scattering at different energies. The calculations have been done using the two-nucleon AV18 potential [20] with and without the three-nucleon URIX force [21]. The results are given at nine different energies in the range $5\ \mathrm{MeV}\leqslant E_{\mathrm{lab}}\leqslant 28\ \mathrm{MeV}$. It has to be noted that, disregarding small corrections, $E_{\mathrm{c.m.}}=\frac{2}{3}E_N$ $(\frac{1}{3}E_d)$, where E_N (E_d) is the nucleon (deuteron) incident energy and in the following we define $E_{\mathrm{lab}}\equiv E_N$. The highest energy considered here is $E_d=56$ MeV ($E_{\mathrm{lab}}=28$ MeV) at which the deuteron analyzing powers are available [22]. Just above the DBT, deuteron vector and tensor analyzing powers are available at $E_{\mathrm{lab}}=5$ MeV [23]. For $E_{\mathrm{lab}}\leqslant 18$ MeV differential cross sections, proton, and deuteron analyzing powers have been measured at several energies [24]. In Ref. [25] differential cross section as well as vector and tensor observables have been measured between $8.5\ \mathrm{MeV}\leqslant E_{\mathrm{lab}}\leqslant 22.7$ MeV, though data for T_{21} are missing at some energies.

The paper is organized as follows. In Sec. II the Kohn variational principle is reviewed. In Sec. III the numerical solution of the related differential equations are compared to previous results. Cross sections and observables are compared to the data in Sec. IV, and the conclusions are given in the last section.

II. THE KOHN VARIATIONAL PRINCIPLE ABOVE THE DEUTERON BREAKUP THRESHOLD

In the literature several investigations regarding the validity of the KVP above the DBT can be found, starting with the works of Nuttall [26] and Merkuriev [27], where the discussion, however, was limited to the n-d reaction. In the work of Rosenberg [28] a first attempt to deal with charged particles has been made. The first extensive demonstration of the applicability of the principle to the p-d collision has been given in Ref. [2]. The main result derived in Ref. [2] is that the effect of the Coulomb interaction can be taken into account in such a way that the form of the principle remains unchanged when the energy goes from below to above the DBT. Below the DBT the collision matrix is unitary and the problem can be formulated in terms of the real reactance matrix (K matrix). Above the DBT the elastic part of the collision matrix is no longer unitary and the formulation in terms of the S matrix, the complex form of the KVP, is convenient. Referring to Ref. [2] for details, a brief description of the method is given below. The scattering wave function (WF) Ψ is written as the sum of two terms:

$$\Psi=\Psi_C+\Psi_A. \tag{1}$$

The first term Ψ_C describes the system when the three-nucleons are close to each other. For large interparticle separations and energies below the DBT it goes to zero, whereas for higher energies it must reproduce a three outgoing particle state. It is written as a sum of three Faddeev-like amplitudes corresponding to the three cyclic permutations of the particle indices 1,2,3. Each amplitude $\Psi_C(\mathbf{x}_i,\mathbf{y}_i)$, where $\mathbf{x}_i,\mathbf{y}_i$ are the Jacobi coordinates corresponding to the ith permutation, has total angular momentum JJ_z and total isospin TT_z and is decomposed into channels using LS coupling, namely,

$$\Psi_C(\mathbf{x}_i,\mathbf{y}_i)=\sum_{\alpha=1}^{N_c}\phi_\alpha(x_i,y_i)\mathcal{Y}_\alpha(jk,i), \tag{2}$$

$$\mathcal{Y}_\alpha(jk,i)=\{[Y_{l_\alpha}(\hat{x}_i)Y_{L_\alpha}(\hat{y}_i)]_{\Lambda_\alpha}[s_\alpha^{jk}s_\alpha^i]_{S_\alpha}\}_{JJ_z}[t_\alpha^{jk}t_\alpha^i]_{TT_z}, \tag{3}$$

where x_i,y_i are the moduli of the Jacobi coordinates and $\mathcal{Y}_\alpha$ is the angular-spin-isospin function for each channel. The maximum number of channels considered in the expansion is N_c. The two-dimensional amplitude ϕ_α is expanded in terms of the PHH basis

$$\phi_\alpha(x_i,y_i)=\rho^{-5/2}f_\alpha(x_i)\left[\sum_K u_K^\alpha(\rho)\,{}^{(2)}P_K^{l_\alpha,L_\alpha}(\phi_i)\right], \tag{4}$$

where the hyperspherical variables, the hyperradius ρ and the hyperangle ϕ_i, are defined by the relations $x_i=\rho\cos\phi_i$ and $y_i=\rho\sin\phi_i$. The factor ${}^{(2)}P_K^{l,L}(\phi)$ is a hyperspherical polynomial and $f_\alpha(x_i)$ is a pair correlation function introduced to accelerate the convergence of the expansion. For small values of the interparticle distance $f_\alpha(x_i)$ is regulated by the NN interaction whereas for large separations the correlation function is chosen to satisfy $f_\alpha(x_i)\rightarrow 1$ [13].

The second term, Ψ_A, in the variational wave function of Eq. (1) describes the asymptotic motion of a deuteron relative to the third nucleon. It can also be written as a sum of three amplitudes with the generic one having the form

$$\Omega^{\lambda}_{LSJ}(\mathbf{x}_i,\mathbf{y}_i)=\sum_{l_\alpha=0,2} w_{l_\alpha}(x_i)\mathcal{R}^{\lambda}_{L}(y_i) \times\{[[Y_{l_\alpha}(\hat{x}_i)s^{jk}_{\alpha}]_1 s^{i}]_S Y_L(\hat{y}_i)\}_{JJ_z}[t^{jk}_{\alpha}t^{i}]_{TT_z}, \tag{5}$$

where $w_{l_\alpha}(x_i)$ is the deuteron WF component in the state $l_\alpha=0,2$. In addition, $s^{jk}_{\alpha}=1, t^{jk}_{\alpha}=0$ and L is the relative angular momentum of the deuteron and the incident nucleon. The superscript λ indicates the regular ($\lambda\equiv R$) or the irregular ($\lambda\equiv I$) solution. In the p-d(n-d) case, the functions $\mathcal{R}^{\lambda}$ are related to the regular or irregular Coulomb (spherical Bessel) functions. The functions Ω^{λ} can be combined to form a general asymptotic state

$$\Omega^{+}_{LSJ}(\mathbf{x}_i,\mathbf{y}_i)=\Omega^{0}_{LSJ}(\mathbf{x}_i,\mathbf{y}_i)+\sum_{L'S'} {}^{J}\mathcal{L}^{SS'}_{LL'}\Omega^{1}_{L'S'J}(\mathbf{x}_i,\mathbf{y}_i), \tag{6}$$

where

$$\Omega^{0}_{LSJ}(\mathbf{x}_i,\mathbf{y}_i)=u_{00}\Omega^{R}_{LSJ}(\mathbf{x}_i,\mathbf{y}_i)+u_{01}\Omega^{I}_{LSJ}(\mathbf{x}_i,\mathbf{y}_i), \tag{7}$$

$$\Omega^{1}_{LSJ}(\mathbf{x}_i,\mathbf{y}_i)=u_{10}\Omega^{R}_{LSJ}(\mathbf{x}_i,\mathbf{y}_i)+u_{11}\Omega^{I}_{LSJ}(\mathbf{x}_i,\mathbf{y}_i). \tag{8}$$

The matrix elements u_{ij} can be selected according to the four different choices of the matrix $\mathcal{L}=K$ matrix, K^{-1} matrix, S matrix, or T matrix. A general three-nucleon scattering WF for an incident state with relative angular momentum L, spin S and total angular momentum J is

$$\Psi^{+}_{LSJ}=\sum_{i=1,3}[\Psi_C(\mathbf{x}_i,\mathbf{y}_i)+\Omega^{+}_{LSJ}(\mathbf{x}_i,\mathbf{y}_i)], \tag{9}$$

and its complex conjugate is Ψ^{-}_{LSJ}. A variational estimate of the trial parameters in the WF Ψ^{+}_{LSJ} can be obtained by requiring, in accordance with the generalized KVP, that the functional

$$[{}^{J}\mathcal{L}^{SS'}_{LL'}]={}^{J}\mathcal{L}^{SS'}_{LL'}-\frac{2}{\det(u)}\langle\Psi^{-}_{LSJ}|H-E|\Psi^{+}_{L'S'J}\rangle \tag{10}$$

be stationary. Below the DBT due to the unitarity of the S matrix, the four forms for the $\mathcal{L}$ matrix are equivalent. However, it was shown that when the complex form of the principle is used, there is a considerable reduction of numerical instabilities [29]. Applications of the complex KVP for N-d scattering (below the DBT) can be found in Ref. [30]. Above the DBT it is convenient to formulate the variational principle in terms of the S matrix. Accordingly, we get the following functional:

$$[{}^{J}S^{SS'}_{LL'}]={}^{J}S^{SS'}_{LL'}+i\langle\Psi^{-}_{LSJ}|H-E|\Psi^{+}_{L'S'J}\rangle. \tag{11}$$

The variation of the functional with respect to the hyperradial functions $u^{\alpha}_{K}(\rho)$ leads to the following set of coupled equations (hereafter named SE1):

$$\sum_{\alpha',k'}\left[A^{\alpha\alpha'}_{kk'}(\rho)\frac{d^2}{d\rho^2}+B^{\alpha\alpha'}_{kk'}(\rho)\frac{d}{d\rho}+C^{\alpha\alpha'}_{kk'}(\rho)+\frac{M_N}{\hbar^2}E\,N^{\alpha\alpha'}_{kk'}(\rho)\right]u^{\alpha'}_{k'}(\rho)=D^{\lambda}_{\alpha k}(\rho). \tag{12}$$

For each asymptotic state ${}^{(2S+1)}L_J$ two different inhomogeneous terms are constructed corresponding to the asymptotic Ω^{λ}_{LSJ} functions with $\lambda\equiv 0,1$. Accordingly, two sets of solutions are obtained and combined to minimize the functional (11) with respect to the S matrix elements. This is the first order solution, the second order estimate of the S matrix is obtained after replacing the first order solution in Eq. (11) [15,30].

In order to solve the system SE1 appropriate boundary conditions must be specified for the hyperradial functions. For energies below the DBT they go to zero when $\rho\to\infty$, whereas above the DBT energy they asymptotically describe the breakup configuration. The boundary conditions to be applied in this case have been discussed in Refs. [2,31] and are briefly illustrated below. To simplify the notation let us label the basis elements with the index $\mu\equiv[\alpha,K]$, and introduce the following completely antisymmetric correlated spin-isospin-hyperspherical basis elements

$$\mathcal{P}_{\mu}(\rho,\Omega)=\sum_{i=1}^{3} f_{\alpha}(x_i)\,{}^{(2)}P^{l_\alpha,L_\alpha}_{K}(\phi_i)\mathcal{Y}_{\alpha}(jk,i), \tag{13}$$

which depend on ρ through the correlation factor and form a nonorthogonal basis. In terms of the $\mathcal{P}_{\mu}(\rho,\Omega)$ the internal part is written as

$$\Psi_C=\rho^{-5/2}\sum_{\mu=1}^{N_m} u_{\mu}(\rho)\mathcal{P}_{\mu}(\rho,\Omega), \tag{14}$$

with N_m the total number of basis functions considered. The ''uncorrelated'' basis elements $\mathcal{P}^{0}_{\mu}(\Omega)$ are obtained from Eq. (13) by setting all the correlation functions $f_{\alpha}(x_i)=1$. It is important to note that the elements $\mathcal{P}^{0}_{\mu}(\Omega)$ do not form an orthogonal basis, as has been discussed in Ref. [32] where the standard hyperspherical harmonic (HH) basis has been used to calculate the three-nucleon bound state. Those basis elements having the same grand-angular quantum number $G_{\mu}=l_{\alpha}+L_{\alpha}+2K$, the same Λ_{α} and S_{α}, but belonging to different channels, are not orthogonal to each others. Moreover, some of them are linearly dependent. In Ref. [32] such states have been identified and removed from the expansion used to describe the triton bound state.

In the present case, the basis elements $\mathcal{P}_{\mu}(\rho\to\infty,\Omega)$ reduce to the uncorrelated ones $\mathcal{P}^{0}_{\mu}(\Omega)$ in the asymptotic region since $f_{\alpha}(x)\to 1$ for large interparticle distances. Therefore, it appears useful to combine the correlated basis (13) in order to define a new basis with the property of being orthonormal when $\rho\to\infty$. This can be readily accomplished by noting that the matrix elements of the norm N behave as

$$N_{\mu\mu'}(\rho)=\int d\Omega\, \mathcal{P}_\mu(\rho,\Omega)^\dagger \mathcal{P}_{\mu'}(\rho,\Omega) \rightarrow N^{(0)}_{\mu\mu'}+\frac{N^{(3)}_{\mu\mu'}}{\rho^3}+\mathcal{O}(1/\rho^5), \quad \text{for } \rho\rightarrow\infty, \tag{15}$$

where, in particular,

$$N^{(0)}_{\mu\mu'}=\int d\Omega\, \mathcal{P}^0_\mu(\Omega)^\dagger \mathcal{P}^0_{\mu'}(\Omega). \tag{16}$$

Let us define a matrix U such that the matrix $U^t N^{(0)} U=\mathcal{N}$ is diagonal with diagonal elements $\mathcal{N}_\mu$ either 1 or 0. The values $\mathcal{N}_\mu=0$ correspond to states $\mathcal{P}^0_\mu(\Omega)$ that depend linearly on others. New uncorrelated and correlated bases are defined as

$$\mathcal{Q}^0_\mu(\Omega)\equiv\sum_{\mu'=1}^{N_m} U_{\mu'\mu}\mathcal{P}^0_{\mu'}(\Omega),$$

$$\mathcal{Q}_\mu(\rho,\Omega)\equiv\sum_{\mu'=1}^{N_m} U_{\mu'\mu}\mathcal{P}_{\mu'}(\rho,\Omega). \tag{17}$$

The basis functions $\mathcal{Q}_\mu(\rho,\Omega)$ are still not orthogonal for any finite values of ρ. When $\rho\rightarrow\infty$, the elements $\mathcal{Q}_\mu(\rho,\Omega)\rightarrow\mathcal{Q}^0_\mu(\Omega)$. Due to the fact that some of the uncorrelated elements $\mathcal{P}^0_\mu(\Omega)$ are linearly dependent, some elements $\mathcal{Q}^0_\mu(\Omega)$ are identically zero. Therefore, some correlated elements have the property: $\mathcal{Q}_\mu(\rho,\Omega)\rightarrow 0$ as $\rho\rightarrow\infty$. In the following we arrange the new basis in such a way that for values of the index $\mu\leqslant\overline{N}_m$ the eigenvalues of the norm are $\mathcal{N}_\mu=1$ and for $\overline{N}_m+1\leqslant\mu\leqslant N_m$ they are $\mathcal{N}_\mu=0$.

In terms of the new basis, the internal part Ψ_C is simply

$$\Psi_C=\rho^{-5/2}\sum_{\mu=1}^{N_m}\omega_\mu(\rho)\mathcal{Q}_\mu(\rho,\Omega), \tag{18}$$

where the old set of hyperradial functions is related to the new set through the transformation $u_\mu=\Sigma_{\mu'}U_{\mu\mu'}\omega_{\mu'}$. The variation of the functional (10) with respect to the new hyperradial functions $\omega_\mu(\rho)$, which are now the unknown quantities entering into the description of the internal part of the *WF* Ψ_C, leads to a set of inhomogeneous second order differential equations formally equal to SE1, and hereafter called SE2, in which each matrix $X\equiv A,B,C,N$ of Eq. (12) is substituted by $\overline{X}=U^tXU$ and the inhomogeneous term D^λ by $\overline{D}^\lambda=U^tD^\lambda$.

For $\rho\rightarrow\infty$, neglecting terms going to zero faster than ρ^{-2}, the asymptotic expression of SE2 reduces to the form

$$\sum_{\mu'}\left\{-\frac{\hbar^2}{M_N}\left(\frac{d^2}{d\rho^2}-\frac{\mathcal{K}_\mu(\mathcal{K}_\mu+1)}{\rho^2}+Q^2\right)\mathcal{N}_\mu\delta_{\mu,\mu'} + \frac{2\,Q\,\chi_{\mu\mu'}}{\rho}+\mathcal{O}\left(\frac{1}{\rho^3}\right)\right\}\omega_{\mu'}(\rho)=0, \tag{19}$$

where $E=\hbar^2Q^2/M_N$, $\mathcal{K}_\mu=G_\mu+3/2$ and the matrix χ is defined as

$$\chi_{\mu\mu'}=\int d\Omega\, \mathcal{Q}^0_\mu(\Omega)^\dagger\,\hat{\chi}\,\mathcal{Q}^0_{\mu'}(\Omega). \tag{20}$$

The dimensionless operator $\hat{\chi}$ originates from the Coulomb interaction as

$$\hat{\chi}=\frac{M_N}{2\hbar^2Q}\sum_{i=1}^{3}\frac{e^2}{\cos\phi_i}\frac{1+\tau_{j,z}}{2}\frac{1+\tau_{k,z}}{2}. \tag{21}$$

It should be noticed that $\chi_{\mu\mu'}=0$ if $\mu,\mu'>\overline{N}_m$.

In practice, the functions $\omega_\mu(\rho)$ are chosen to be regular at the origin, i.e., $\omega_\mu(0)=0$ and, in accordance with the equations to be satisfied for $\rho\rightarrow\infty$, to have the following behavior ($\mu\leqslant\overline{N}_m$):

$$\omega_\mu(\rho)\rightarrow-\sum_{\mu'=1}^{\overline{N}_m}(e^{-i\hat{\chi}\ln 2Q\rho})_{\mu\mu'}b_{\mu'}e^{iQ\rho}, \tag{22}$$

where $b_{\mu'}$ are unknown coefficients. This form corresponds to the asymptotic behavior of three outgoing particles interacting through the Coulomb potential [33]. In the case of *n-d* scattering ($\chi\equiv 0$) the outgoing solutions evolve as outgoing Hankel functions $H^{(1)}(Q\rho)[\omega_\mu(\rho)\rightarrow-b_\mu e^{iQ\rho}]$.

For values of the index $\mu>\overline{N}_m$ the eigenvalues of the norm are $\mathcal{N}_\mu=0$ and the leading terms in Eq. (19) vanish. So, the asymptotic behavior of these ω_μ functions is governed by the next order terms. A lengthy analysis of the $1/\rho^3$ and $1/\rho^4$ terms for each matrix $X\equiv A,B,C,N$ shows that these functions behave as $e^{i(Q'_\mu\rho-\Sigma_\mu\ln 2Q\rho)}$ where the quantities Q'_μ,Σ_μ are related to the asymptotic expansion of the matrices A,B,C,N. This asymptotic behavior has been obtained neglecting all couplings between the μth equation ($\mu>\overline{N}_m$) and all the others. If couplings up to $1/\rho^4$ are taken into account the quantities Q',Σ become matrices and we have ($\mu>\overline{N}_m$)

$$\omega_\mu(\rho)\rightarrow-\sum_{\mu'=1}^{N_m}[e^{(iQ'\rho-\Sigma\ln 2Q\rho)}]_{\mu\mu'}c_{\mu'}, \tag{23}$$

where the $c_{\mu'}$ are unknown coefficients. Previously we have shown that, for $\mu>\overline{N}_m$, the elements $\mathcal{Q}_\mu\rightarrow 0$ as $\rho\rightarrow\infty$. The specific form of the (complex) matrix Σ is such that in all cases $\omega_\mu\mathcal{Q}_\mu\rightarrow 0$ as $\rho\rightarrow\infty$. Accordingly, the states with $\mu>\overline{N}_m$ do not contribute to the outgoing flux.

In Ref. [31] the set of equations SE2 has been solved numerically by choosing a grid of values for the hyperradius from the origin up to a certain value ρ_0. The differential operators have been substituted by finite differences in such a way that SE2 reduces to a set of linear equations that can be solved by standard numerical methods. In order to completely determine the problem, boundary conditions must be imposed at $\rho=\rho_0$. To accomplish this, Eq. (19) has been solved for $\rho>\rho_0$ taking into account coupling terms up to ρ^{-4} by an expansion of the functions ω_μ in powers of $1/\rho$ and verifying the outgoing boundary conditions of Eqs. (22),(23). Then, the continuity of the solutions and their first

derivatives has been imposed at the matching radius ρ_0. The value of ρ_0 is not important provided that the asymptotic expression of SE2 is already reached. This condition is well verified for values of the matching radius $\rho_0 \gtrsim 80$–100 fm. However, the functions $\omega_\mu(\rho)$ show an oscillatory behavior outside the range of the potential, typically for hyperradial values $\rho > 30$ fm. Therefore a large number of grid points were necessary to obtain stable solutions. Thus, in Ref. [31] the calculation of N-d scattering states above the DBT was restricted to a simplified interparticle potential, namely, an s-wave interaction. In such a case the number of coupled equations to be considered was sufficiently small. When realistic NN interactions are considered the number of coupled equations to take into account increases considerably. As a consequence, the dimension of the matrices after the reduction of derivatives to finite differences can be quite large. In order to keep the dimension of the matrices low, an alternative method of solution in the region $\rho \leqslant \rho_0$ is to expand the hyperradial functions in terms of Laguerre polynomials [1] plus an auxiliary function

$$\omega_\mu(\rho) = \rho^{5/2} \sum_{m=0}^{M} A_\mu^m L_m^{(5)}(z) \exp\left(-\frac{z}{2}\right) + A_\mu^{M+1} \overline{\omega}_\mu(\rho), \tag{24}$$

where $z = \gamma\rho$ and γ is a nonlinear parameter. The linear parameters A_μ^m $(m = 0, \ldots, M+1)$ are determined by the variational procedure. The functions defined above are matched to the outgoing solutions of Eq. (19) at $\rho = \rho_0$.

The inclusion of the auxiliary functions $\overline{\omega}_\mu(\rho)$ defined in Eq. (24) is useful for reproducing the oscillatory behavior shown by the hyperradial functions for $\rho \gtrsim 30$ fm. Otherwise a rather large number M of polynomials should be included in the expansion. A convenient choice is to take them as the solutions of a one dimensional differential equation corresponding to the μth equation of SE2

$$\left[\overline{A}_{\mu\mu}(\rho)\frac{d^2}{d\rho^2} + \overline{B}_{\mu\mu}(\rho)\frac{d}{d\rho} + \overline{C}_{\mu\mu}(\rho) + Q^2\overline{N}_{\mu\mu}(\rho)\right]\overline{\omega}_\mu(\rho) = \overline{D}_\mu^\lambda(\rho). \tag{25}$$

The functions $\overline{\omega}_\mu$ are chosen to be regular at the origin and they are matched to the solutions of Eq. (19) which have been obtained through an expansion in inverse powers of ρ as has been previously discussed. For $\mu > \overline{N}_m$ the matching at ρ_0 has been done disregarding the couplings between the different equations in the region $\rho > \rho_0$, i.e., $\overline{\omega}_\mu(\rho) \to e^{i(Q'_\mu\rho - \Sigma_\mu \ln 2Q\rho)}$. As stated before, these states do not contribute to the outgoing flux and their importance in the construction of the scattering state diminishes very rapidly for large values of ρ. The approximation introduced for $\rho > \rho_0$ in the application of the boundary condition to the states with $\mu > \overline{N}_m$ has been checked by increasing the value of the matching radius. In the cases considered here the solutions obtained for the S matrix show a complete stability for values of the matching radius $\rho_0 > 100$ fm.

Let us define $|\mu, m\rangle$ to be a correlated totally antisymmetric element of the expansion basis. Here μ indicates the correlated HH state $\mathcal{Q}_\mu(\rho, \Omega)$ and $m = 1, \ldots, M$ indicates the Laguerre polynomial $L_m^{(5)}(z)$ or, for $m = M+1$, the auxiliary function $\overline{\omega}_\mu$. In terms of these basis elements the internal part of the wave function is

$$\Psi_C = \sum_{\mu,m} A_\mu^m |\mu, m\rangle. \tag{26}$$

The variation of the functional $[{}^J S_{LL}^{SS}]$ with respect to the linear parameters leads to the following set of linear equations:

$$\sum_{\mu',m'} A_{\mu'}^{m'} \langle \mu, m | H - E | \mu', m' \rangle = D_{\mu,m}^\lambda, \tag{27}$$

where the inhomogeneous term is

$$D_{\mu,m}^\lambda = \sum_j \langle \mu, m | H - E | \Omega_{LSJ}^\lambda(\mathbf{x}_i, \mathbf{y}_i) \rangle. \tag{28}$$

The first order solution of the S matrix is obtained solving the algebraic equations

$$\sum_{L''S''} {}^J S_{LL'}^{SS'} X_{L'L''}^{S'S''} = Y_{LL'}^{SS'}, \tag{29}$$

with the coefficients X and Y defined to be

$$X_{LL'}^{SS'} = \langle \Omega_{LSJ}^1 + \Psi_{LSJ}^1 | H - E | \Omega_{LSJ}^1 \rangle,$$

$$Y_{LL'}^{SS'} = \langle \Omega_{LSJ}^0 + \Psi_{LSJ}^0 | H - E | \Omega_{LSJ}^0 \rangle, \tag{30}$$

where Ψ_{LSJ}^λ is constructed using the solution of Eq. (27) with the corresponding inhomogeneous term. The second order estimate $[{}^J S_{LL'}^{SS'}]$ is obtained replacing the first order solution in Eq. (11).

In addition to the asymptotic form of the wave function discussed above, there is a region of the configuration space in which a neutron and a proton continue to interact in a $l = 0$ zero energy relative state, both nucleons being far from the third one. This specific configuration has been discussed by Merkuriev for the first time [27,33], in a more complete form by Alt and Mukhamedzhanov [34] and recently by Friar and Payne [35]. Though this asymptotic term gives an important contribution to the breakup amplitude when $\phi_i \to \pi/2$, its effect in the description of the elastic S matrix elements using the KVP is extremely small. In fact, this region of the configuration space belongs to the regions $[\Omega_i]$ and $[\Omega_{t,i}]$ defined in Ref. [2], that have been shown to give a negligible contribution to the error term $\langle \epsilon | H - E | \epsilon \rangle$ entering the calculation of the elastic S matrix using the KVP (ϵ represents the difference between the exact and the trial

wave functions). In the present work the term in which a neutron and a proton are in a $l=0$ relative state is implicitly included in the Ψ_C term and constructed through the expansion in terms of PHH basis. A truncation of the basis is performed after a complete stabilization of the second order $[{}^J S_{LL'}^{SS'}]$ elements. At the same time, the breakup amplitude is obtained at the first order in terms of the coefficients b_μ defined in Eq. (22). The convergence of the breakup amplitude has been found to be very slow when $\phi_i \to \pi/2$ and this fact is related to the difficulties of the expansion to reproduce the aforementioned term in the regions $[\Omega_i]$ and $[\Omega_{t,i}]$. The application of the KVP to describe the breakup amplitude will be given in a forthcoming paper and will not be discussed any further in the present work.

Finally, due to flux conservation the following condition has to be satisfied between the matrix elements of the elastic S matrix and the coefficients of the outgoing breakup waves:

$$\sum_{S'L'} |{}^J S_{LL'}^{SS'}|^2 + \sum_\mu |b_\mu|^2 = 1. \tag{31}$$

The coefficients b_μ, which are defined in Eq. (22), are the linear parameters A_μ^{M+1} of Eq. (24). The above relation allows the calculation of the total breakup cross section from the elastic S-matrix elements, as has been recently discussed in Ref. [36].

III. NUMERICAL RESULTS

In order to study the solution of Eq. (12) by means of the expansion given in Eq. (24), we have first calculated the phase-shift and inelasticity parameters for n-d and p-d scattering using the spin-dependent s-wave potential of Malfliet and Tjon. The results are presented in Table I for two energy values $E_{\rm lab}=14.1$ and 42.0 MeV. The calculations have been done using $N_\alpha=8$ hyperspherical polynomials per channel, as in the case already studied in Ref. [31] where the set of equations SE1 was solved using the finite difference technique. Moreover, since the potential is central, the phase shifts ${}^{2S+1}\delta_L$ and inelasticities ${}^{2S+1}\eta_L$ do not depend on the total angular momentum J. Only the case $L=0$ has been considered and the results are given in Table I for increasing values of the number of Laguerre polynomials M. For the sake of comparison the results of Ref. [31] are reported as well as the benchmark results of Ref. [37] obtained by solving the Faddeev equations in configuration space (Los Alamos group) and momentum space (Bochum group). We observe a very fast convergence with M and, in general, 16 to 20 polynomials are enough to obtain the phase shift and mixing parameters with four digit accuracy. With the number of Laguerre polynomials that has been taken into account a very low dependence on the nonlinear parameter γ has been observed. In fact the results reported here do not change for variations of the parameter in the range 1.5 fm$^{-1} \leqslant \gamma \leqslant$ 2.5 fm^{-1}. Moreover, the dimension of the matrices involved in the solution is one order of magnitude smaller than that used in Ref. [31].

The case of realistic interactions has been considered in Refs. [1,2] where the AV18 interaction has been used to calculate p-d scattering at $E_{\rm lab}=5$ and 10 MeV. In particular, in Ref. [2] the convergence of the phase shift and mixing parameters for the state $J=1/2^+$ has been studied by increasing the number of angular-spin-isospin channels. The convention discussed in Ref. [38] has been adopted in the parametrization of the S matrix in terms of phase-shift and mixing parameters. In order to illustrate the variation of these parameters with energy the doublet and quartet S, P, and D phases, denoted as ${}^{2S+1}L_J$, are reported in Fig. 1 as well as the mixing parameters $\eta_{1/2+}$, $\eta_{3/2+}$, $\epsilon_{1/2-}$, and $\epsilon_{3/2-}$. Both the real and imaginary parts are shown. It is interesting to notice that the splitting in the real part of the phases with equal spin S and angular momentum L but different J, increases with energy. Conversely, the imaginary parts of the phases, which are related to the inelasticity of a state with a given value of J, reveal a tiny splitting. After summing all the contributions, the total breakup cross section can be obtained, as is discussed in the next section.

IV. p-d CROSS SECTIONS

The calculation of scattering observables using the present variational technique is based on the estimate of the elastic S matrix for all states with $J \leqslant J_{\rm max}$. Each observable is obtained from a trace operation after the evaluation of the transition matrix, following the formalism of Seyler [39]. The value of $J_{\rm max}$ has been chosen by requiring that partial waves with $J > J_{\rm max}$ give negligible contributions to all the observables considered. In the present work results for cross sections, vector and tensor analyzing powers up to $E_{\rm lab}=28$ MeV are presented, and correspondingly the value $J_{\rm max}=19/2$ has been found to be appropriate.

Let us start with the analysis of the p-d cross sections. For p-d scattering the total breakup cross section accounts for all possible configurations in which all three particles are moving away from each other. Its expression can be given in terms of the elastic S matrix [36]

$$\sigma_b(p\text{-}d) = \frac{\pi}{k^2}\frac{1}{6}\sum_J (2J+1)\,\mathrm{tr}\{I_J - S_J S_J^\dagger\}, \tag{32}$$

where $k^2 = 2\mu E_{cm}/\hbar^2$ (μ is the nucleon-deuteron reduced mass) and I_J is the 3×3 identity matrix, except for $J=1/2$ which is the 2×2 identity matrix. The quantity S_J is the elastic S matrix for the state J. The sum runs over all possible values of J and parity (the sum over the two parities is implied). In principle the sum runs from $J=0$ to infinity, but there is a rapid convergence since each S_J matrix becomes closer to unitary as J increases. In Fig. 2 the theoretical prediction for $\sigma_b(p\text{-}d)$ is given together with the two sets of data available in the literature. The first data set corresponds to energies just above the DBT [40] whereas the second starts at 20 MeV [41]. The solid line is the AV18 prediction and is found to be in reasonable agreement with both sets of data. The inclusion of the URIX potential does not produce appreciable modifications and both results, with and without the inclusion of the 3NF, nearly coincide. The low sensitivity to the 3NF can be understood by noticing that the contribution to σ_b comes from a balance between the spin factor

TABLE I. Phase-shift and mixing parameters for different values of the number M of the Laguerre polynomials used in the expansion of the hyperradial functions. The s-wave potential of Malfliet and Tjon has been considered.

		n-d at $E_n=14.1$ MeV		
M	$^2\delta_0$	$^2\eta_0$	$^4\delta_0$	$^4\eta_0$
4	104.44	0.4672	68.993	0.9669
8	105.33	0.4663	68.963	0.9774
12	105.42	0.4658	68.951	0.9781
16	105.49	0.4646	68.952	0.9782
20	105.48	0.4648	68.952	0.9782
24	105.48	0.4649	68.952	0.9782
28	105.48	0.4649	68.952	0.9782
Ref. [27]	105.50	0.4649	68.95	0.9782
Los Alamos	105.48	0.4648	68.95	0.9782
Bochum	105.50	0.4649	68.96	0.9782
		p-d at $E_p=14.1$ MeV		
4	107.37	0.5006	71.665	0.9654
8	108.34	0.4984	72.615	0.9799
12	108.42	0.4988	72.602	0.9794
16	108.45	0.4984	72.602	0.9795
20	108.43	0.4984	72.604	0.9795
24	108.44	0.4984	72.604	0.9795
28	108.44	0.4984	72.604	0.9795
Ref. [27]	108.43	0.4984	72.604	0.9795
		n-d at $E_n=42.0$ MeV		
M	$^2\delta_0$	$^2\eta_0$	$^4\delta_0$	$^4\eta_0$
4	42.198	0.4575	38.218	0.8917
8	41.818	0.4934	37.680	0.9028
12	41.147	0.5009	37.607	0.9016
16	41.271	0.5010	37.724	0.9027
20	41.332	0.5020	37.723	0.9031
24	41.340	0.5022	37.722	0.9033
28	41.341	0.5022	37.722	0.9033
Ref. [27]	41.33	0.5026	37.71	0.9034
Los Alamos	41.34	0.5024	37.71	0.9035
Bochum	41.37	0.5022	37.71	0.9033
		p-d at $E_n=42.0$ MeV		
M	$^2\delta_0$	$^2\eta_0$	$^4\delta_0$	$^4\eta_0$
4	38.048	0.3988	39.937	0.8738
8	44.701	0.4961	40.554	0.9103
12	43.479	0.5079	39.844	0.9011
16	43.618	0.5059	39.934	0.9036
20	43.660	0.5055	39.947	0.9043
24	43.667	0.5056	39.947	0.9046
28	43.667	0.5056	39.947	0.9046
Ref. [27]	43.65	0.5058	39.94	0.9047

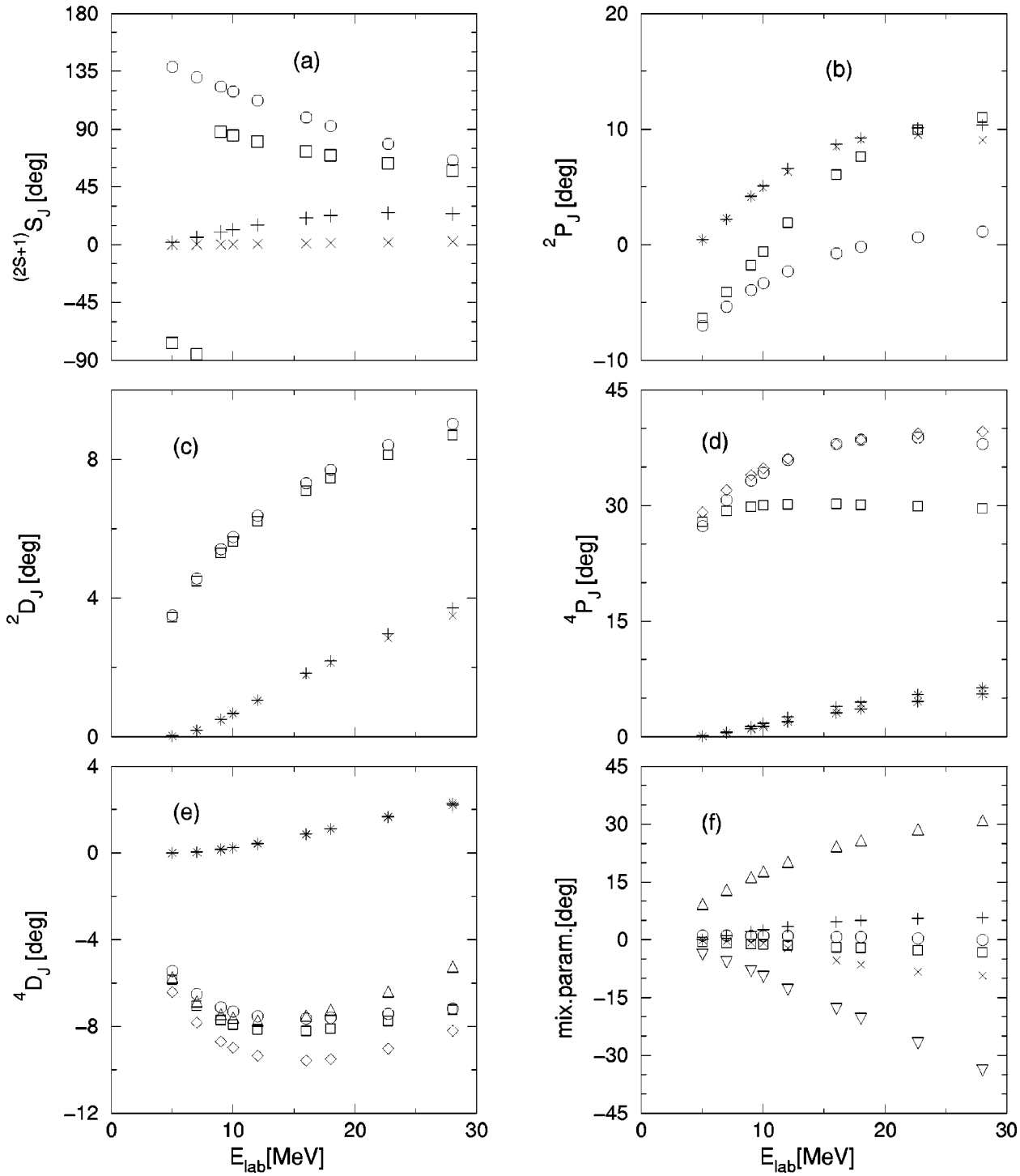

FIG. 1. Phase-shift and mixing parameters (in degrees) as a function of energy. (a) $^2S_{1/2}$ and $^4S_{3/2}$, their real and imaginary parts are indicated by ($\bigcirc$,+) and ($\square$,$\times$), respectively. (b) $^2P_{1/2}$ and $^2P_{3/2}$, their real and imaginary parts are indicated by ($\bigcirc$,+) and ($\square$,$\times$), respectively. (c) $^2D_{3/2}$ and $^2D_{5/2}$, their real and imaginary parts are indicated by ($\bigcirc$,+) and ($\square$,$\times$), respectively. (d) $^4P_{1/2}$, $^4P_{3/2}$, and $^4P_{5/2}$, their real and imaginary parts are indicated by ($\bigcirc$,+), ($\square$,$\times$), and ($\diamond$,*), respectively. (e) $^4D_{1/2}$, $^4D_{3/2}$, $^4D_{5/2}$, and $^4D_{7/2}$, their real parts are indicated by $\bigcirc$, $\square$, $\diamond$, and $\triangle$, respectively. Only the imaginary part of $^4D_{1/2}$ is given (+). (f) Mixing parameters $\eta_{1/2+}$, $\eta_{3/2+}$, $\epsilon_{1/2-}$, and $\epsilon_{3/2-}$, their real parts are indicated by $\bigcirc$, $\square$, $\triangle$, and $\triangledown$, respectively. The imaginary parts of $\epsilon_{1/2-}$ and $\epsilon_{3/2-}$ are indicated by + and $\times$, respectively. The imaginary parts of $\eta_{1/2+}$ and $\eta_{3/2+}$ are close to zero and are not shown.

$2J+1$ and the quantity $\mathrm{tr}\{I_J - S_J S_J^\dagger\}$ which can be considered as a measurement of the inelasticity of the state (divided by $\mathrm{tr}\{I_J\}$). Above 5 MeV the state $J=3/2^-$ gives by far the main contribution to the observable [36]. The state $J=1/2^+$, which is appreciably modified by the 3NF, has the largest inelasticity, but due to a small spin factor it gives a contribution of the same order as other states that are much less ''inelastic'' and modified slightly by the 3NF. The final result

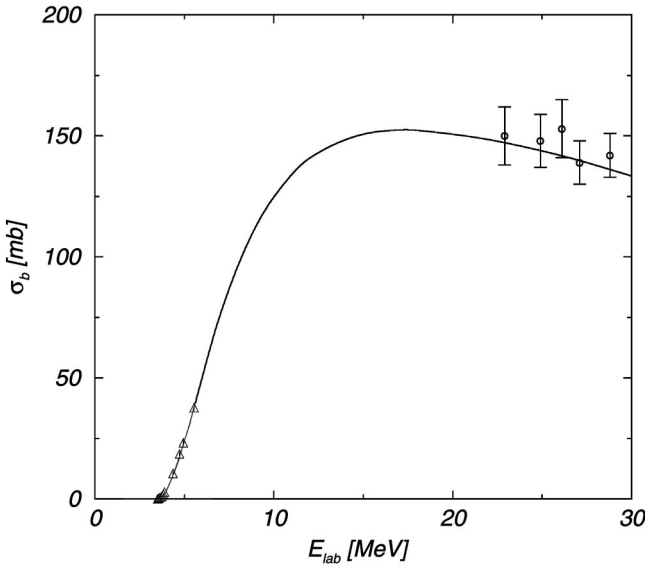

FIG. 2. The p-d total breakup cross section σ_b below 30 MeV calculated using the AV18 interaction. The experimental results of Gibbons and Macklin [40] (open triangles) and Carlson *et al.* [41] (open circles) are given for the sake of comparison.

after summing up all these contributions is that the small (but sizable) effect of the 3NF on $J=1/2+$ has no impact in σ_b.

Regarding the elastic p-d differential cross section, a huge amount of high quality data has been collected during the past years. Low-energy measurements have been taken recently at TUNL at different energy values below $E_{\rm lab}=1$ MeV [10,42,43]. An analysis of the quality in the description of these data has been performed using the AV18 and the AV18+URIX interactions [44,45]. It was shown that 3NF effects can be revealed through a χ^2 analysis of the data. Essentially these effects are related to a correct description of the ^{3}He binding energy. In fact, using the AV18 +URIX interaction it is possible to describe the p-d differential cross section at $E_{\rm lab}=1$, 2, and 3 MeV with a χ^2 per datum (χ^2_N) close to 1. This value increases significantly when the AV18 potential is considered alone. The agreement between the theoretical and experimental differential cross section worsens, though not dramatically, as the energy increases. For example, at $E_{\rm lab}=135$ MeV a value of $\chi^2_N=16.9$ (225.2) was recently obtained with (without) the inclusion of a 3NF [46]. Again the inclusion of a 3NF reduces the χ^2 per datum considerably.

The results obtained for the p-d differential cross section are given in Fig. 3 for nine values of the energy, $E_{\rm lab}=5,7,9,10,12,14,16,18,22.7,28$ MeV. For each energy three curves are shown corresponding to calculations using the AV18 potential (solid line), the AV18+URIX potential (dotted line), and calculations for n-d scattering using the AV18 potential (dashed line). The theoretical predictions are compared to the experimental data of Refs. [24,25,22], with the exception of the calculations at 16 MeV which are compared to data obtained at a slightly different energy (16.5 MeV). The analysis of the results at the different energies shows that 3NF effects are small in this energy range and the AV18 and AV18+URIX curves practically overlap each other. A more quantitative analysis at $E_{\rm lab}=18$ MeV gives $\chi^2_N=11$ using the AV18 interaction and nearly the same value for AV18+URIX. Coulomb effects are mainly observed at forward and backward angles whilst they are strongly reduced at the minimum. Tiny Coulomb effects at the minimum are confirmed by comparing n-d to p-d data, as can be seen in Ref. [3].

As far as the agreement between theory and experiment is concerned, the situation for the differential cross section above the DBT is different when compared to what has been observed below the DBT. As mentioned before, at very low energies the differential cross section can be described with $\chi^2_N\approx 1$ using AV18+URIX, while when the AV18 is used alone a substantially worse result, $\chi^2_N>10$, is obtained. In fact, the AV18 curve remains above the data points all over the angular distribution. As the energy increases the tendency for the AV18 curve is to go below the data at the minimum. This problem is appreciable already at 28 MeV, as can be seen in the last panel of Fig. 3. Around 20 MeV the AV18 +URIX curve starts to rise above the AV18 curve and closer to the data. This effect is clearly shown in Ref. [4] where Faddeev calculations using several NN and 3NF interactions have been compared to the data at 3, 65, 135, and 190 MeV. In the energy range analyzed here we observe that there is one energy, around 18 MeV, where the AV18 and AV18 +URIX curves mostly overlap. In order to analyze further this behavior, in Table II, the values at the minimum of the p-d cross section calculated with AV18 and AV18+URIX are compared to the data. The corresponding values of the AV18 n-d cross section are also given in order to have a quantitative idea of the size of the Coulomb effects.

V. POLARIZATION OBSERVABLES

The vector and tensor analyzing powers are examples of polarization observables. There is a large amount of p-d and d-p data for the vector analyzing powers A_y and iT_{11} as well as for the tensor analyzing powers T_{20}, T_{21}, T_{22}. The study of these observables is important because they are sensible to the noncentral terms of the nuclear interaction. These terms are responsible for small components in the wave function which in general are less known. Therefore, the accuracy shown by the modern interactions when reproducing the vector and tensor analyzing powers in the three-nucleon system gives important information about parts of the nuclear interaction not completely under control. As is well known, in the low-energy region the vector analyzing powers are heavily underpredicted by all modern NN interactions and the origin of this discrepancy is not yet completely understood. Possible ways for solving this puzzle have recently been investigated, based on the inclusion of new terms in the three-nucleon potential [47,48] or on a new NN potential obtained from chiral perturbation theory [49]. These studies represent only a first step in the understanding of the puzzle and further investigations and refinements of the models are needed. A similar underprediction of the proton analyzing power A_y has been found in calculations on p-^{3}He scattering, as was

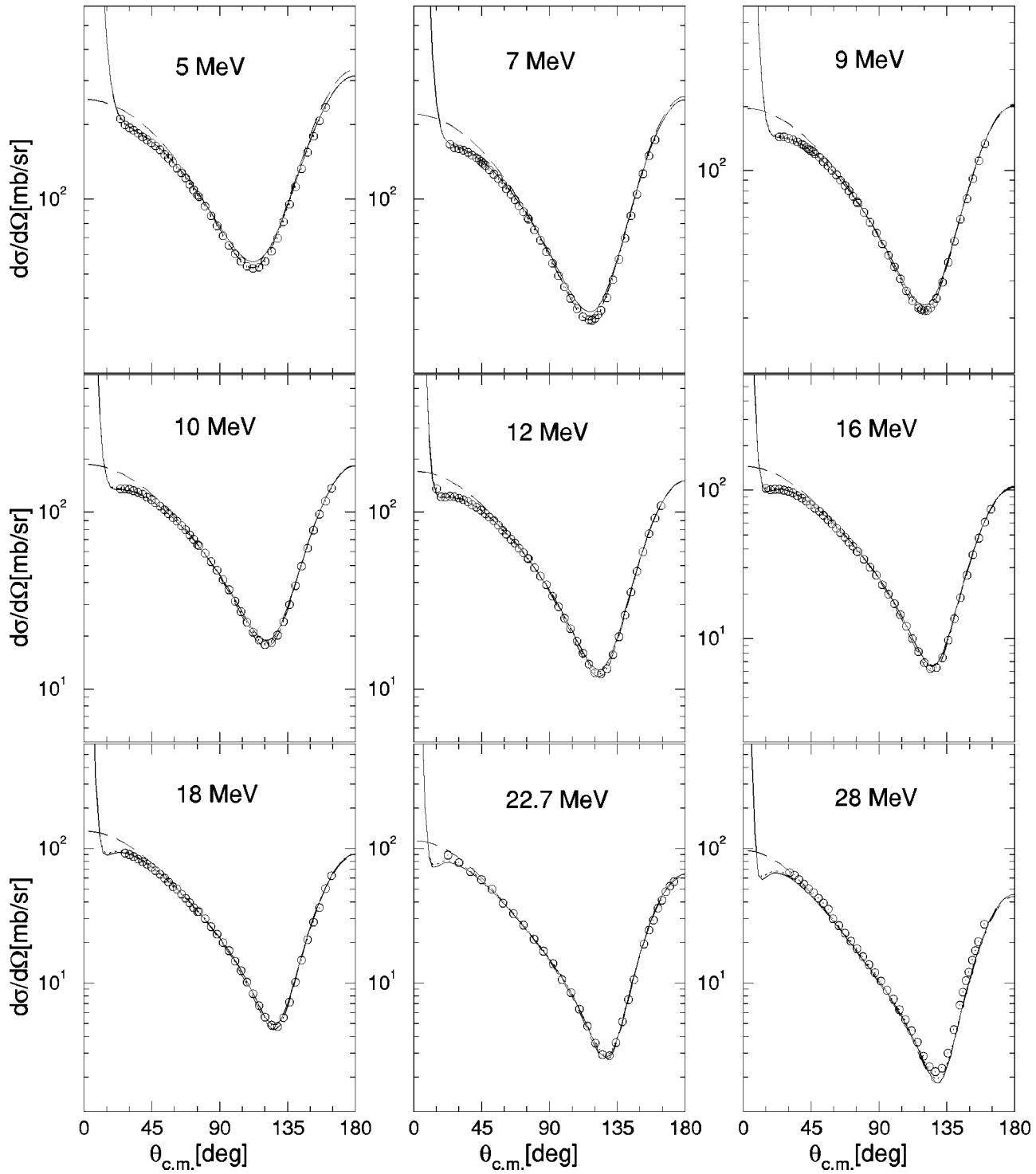

FIG. 3. *N-d* differential cross section up to 28 MeV. Calculations are shown for *p-d* scattering using the AV18 (solid line) and AV18 + UR (dotted line) potentials and for *n-d* scattering using the AV18 potential (dashed line). Data are from Ref. [24] at $E_{\rm lab}$ = 5,7,9,10,12,16,18 MeV, from Ref. [25] at $E_{\rm lab}$ = 22.7 MeV, and from Ref. [22] at $E_{\rm lab}$ = 28 MeV.

recently pointed out [50]. Therefore, a solution to the puzzle should concern both the 3*N* and 4*N* systems.

In the present paper, we will discuss the quality of the description of the vector and tensor polarization observables achieved by the AV18 and the AV18 + URIX interactions in *p-d* scattering up to 28 MeV. In Fig. 4 the results for A_y are given for the same nine energy values given in Fig. 3. The three curves correspond to the *p-d* A_y calculated using AV18 (solid line) and AV18 + URIX (dotted line), and the *n-d* A_y calculated using AV18 (dashed line). The calculations are compared to data from Ref. [24] at $E_{\rm lab}$ = 5,7,9,10,12,16,18 MeV, and from Ref. [25] at $E_{\rm lab}$ = 22.7 MeV. As expected, Coulomb effects are appreciable in all the energy range. Below 18 MeV the effects are appre-

TABLE II. The minimum of the n-d and p-d differential cross sections (in mb/sr) at different energies, calculated using the AV18 and AV18+UR potential models. Experimental data for the p-d cross section are from Refs. [22,24,25,44].

Energy	AV18(n-d)	AV18(p-d)	AV18+UR(p-d)	exp.
1 MeV	148.9	177.5	170.7	170.2 ± 1.3
3 MeV	92.7	96.0	92.3	91.1 ± 0.7
5 MeV	53.1	56.2	53.8	52.7 ± 0.4
7 MeV	32.9	35.3	33.9	32.9 ± 0.2
9 MeV	21.3	23.1	22.1	21.8 ± 0.2
10 MeV	17.3	18.9	18.2	18.0 ± 0.2
12 MeV	11.8	12.8	12.5	12.2 ± 0.1
16 MeV	6.0	6.5	6.4	6.2 ± 0.1
18 MeV	4.5	4.9	4.9	4.7 ± 0.1
22.7 MeV	2.7	2.8	2.9	2.89 ± 0.03
28 MeV	1.8	1.8	1.9	2.19 ± 0.02

ciable at the maximum. Above 18 MeV the shape of A_y changes and a clear minimum appears, where Coulomb effects can be observed. The order of magnitude of these effects is 15%. Instead, 3NF effects are not so important. This is a characteristic of the Urbana potential that modifies the quartet P waves (which produces the main contribution to A_y below 30 MeV) in such a way that there is a cancellation among the different contributions, so the global effect on the observable is small. A similar analysis holds for iT_{11}, shown in Fig. 5, since these two observables have rather similar structures. The calculations for iT_{11} are compared to data from Ref. [24] at $E_{\rm lab}=5,7,9$ MeV, from Ref. [25] at $E_{\rm lab}=10,12,16.5,22.7$ MeV, and from Ref. [22] at $E_{\rm lab}=28$ MeV, taking care again that at 16 MeV the comparison is to data obtained at a slightly different energy (16.5 MeV). As a difference between the proton and deuteron analyzing powers, we observed that Coulomb and 3NF effects are of the same size at the minimum of iT_{11} above 16 MeV.

In Figs. 6–8 the tensor observables T_{20}, T_{21}, T_{22} are given, respectively. As before, the three curves correspond to the p-d T_{ij} calculated using AV18 (solid line) and AV18 +URIX (dotted line), and the n-d T_{ij} calculated using AV18

TABLE III. χ^2 per datum obtained in the description of the vector and tensor analyzing powers at several energies using the AV18 and AV18+UR potentials.

Energy	Potential	A_y	iT_{11}	T_{20}	T_{21}	T_{22}
1 MeV	AV18	276	112	3.5	4.5	2.8
	AV18+UR	190	61	1.0	2.5	0.7
3 MeV	AV18	313	205	4.8	6.7	12
	AV18+UR	271	144	5.4	11	2.4
5 MeV	AV18	211	99	6.8	12	7.8
	AV18+UR	186	59	26	36	1.5
7 MeV	AV18	303	90	19	38	1.9
	AV18+UR	239	56	40	81	4.2
9 MeV	AV18	292	165	42	70	38
	AV18+UR	218	134	63	86	7.2
10 MeV	AV18	288	29	10	6.2	24
	AV18+UR	224	23	13	6.1	7.6
12 MeV	AV18	313	50	19		39
	AV18+UR	227	34	16		22
16 MeV	AV18	296	80	114		70
	AV18+UR	246	61	139		48
18 MeV	AV18	293				
	AV18+UR	250				
22.7 MeV	AV18	78	89	44		24
	AV18+UR	72	61	59		17
28 MeV	AV18		19	10	7.1	11
	AV18+UR		13	10	11	8.5

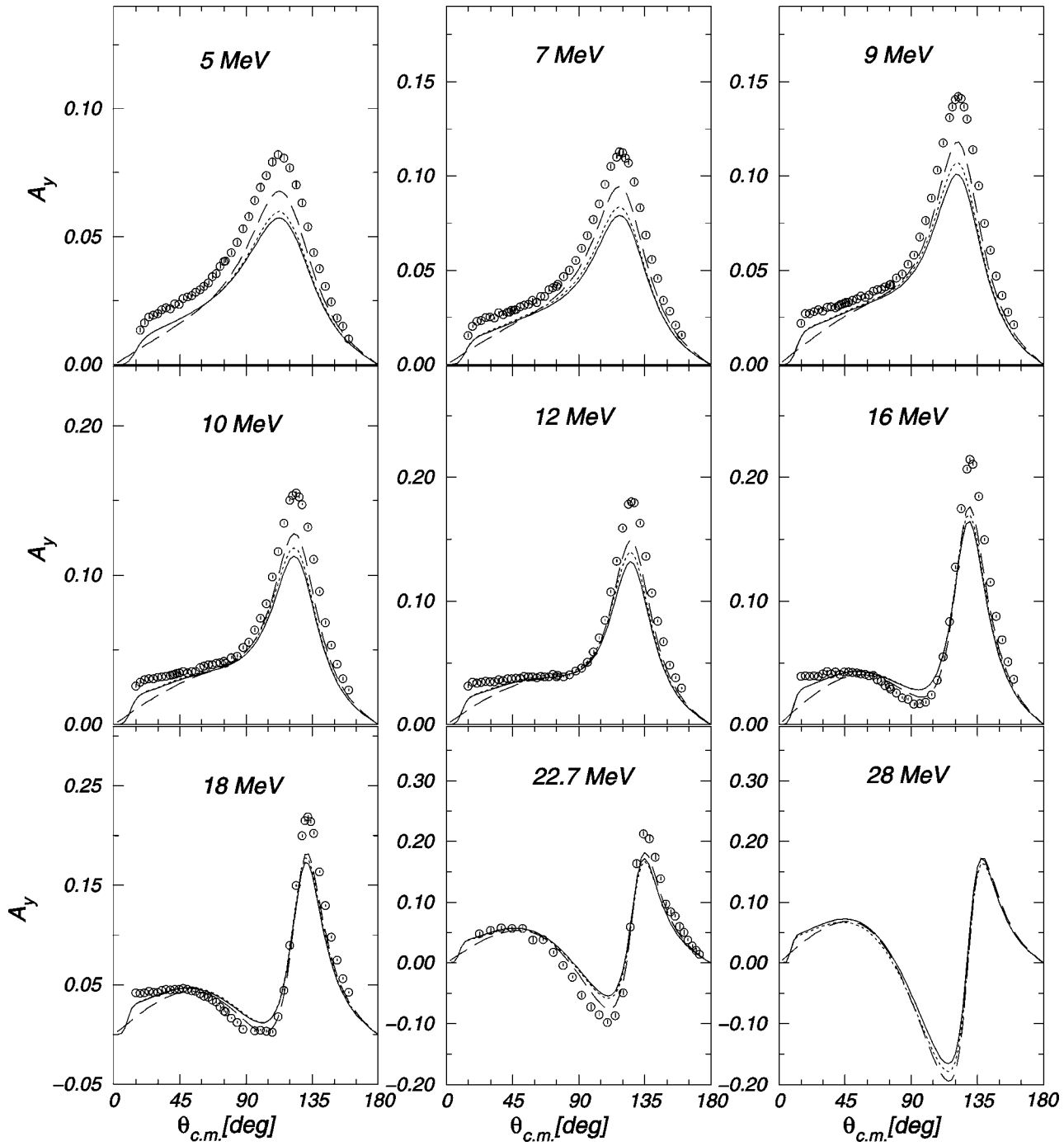

FIG. 4. Nucleon vector analyzing power A_y up to 28 MeV. Calculations are shown for p-d scattering using the AV18 (solid line) and AV18+UR (dotted line) potentials and for n-d scattering using the AV18 potential (dashed line). Data are from Ref. [24] at $E_{\rm lab}$ =5,7,9,10,12,16,18 MeV and from Ref. [25] at $E_{\rm lab}$=22.7 MeV.

(dashed line). The calculations are compared to data from Ref. [24] at $E_{\rm lab}$=5,7,9 MeV, from Ref. [25] at $E_{\rm lab}$ =10,12,16.5,22.7 MeV, and from Ref. [22] at $E_{\rm lab}$ =28 MeV. As a general trend, the agreement with the data for the tensor observables is better than for the vector observables. Coulomb effects are appreciable in the three observables at low energies. As the energy increases the inclusion of the Coulomb interaction in the analysis of the tensor observables is less important, mostly for T_{20} and T_{22}. The case of T_{21} is of particular interest since Coulomb effects are still appreciable at 28 MeV. This observation suggests that comparisons of d-p data to calculations where the Coulomb interaction has been neglected should be done with caution. The effect of the 3NF is somehow contradictory since in some cases its inclusion improves the description of the observables but in other cases it does not. For example, a net improvement is obtained in the description of the minimum of T_{22} below 12 MeV. Also the maximum of T_{20} and T_{21} is

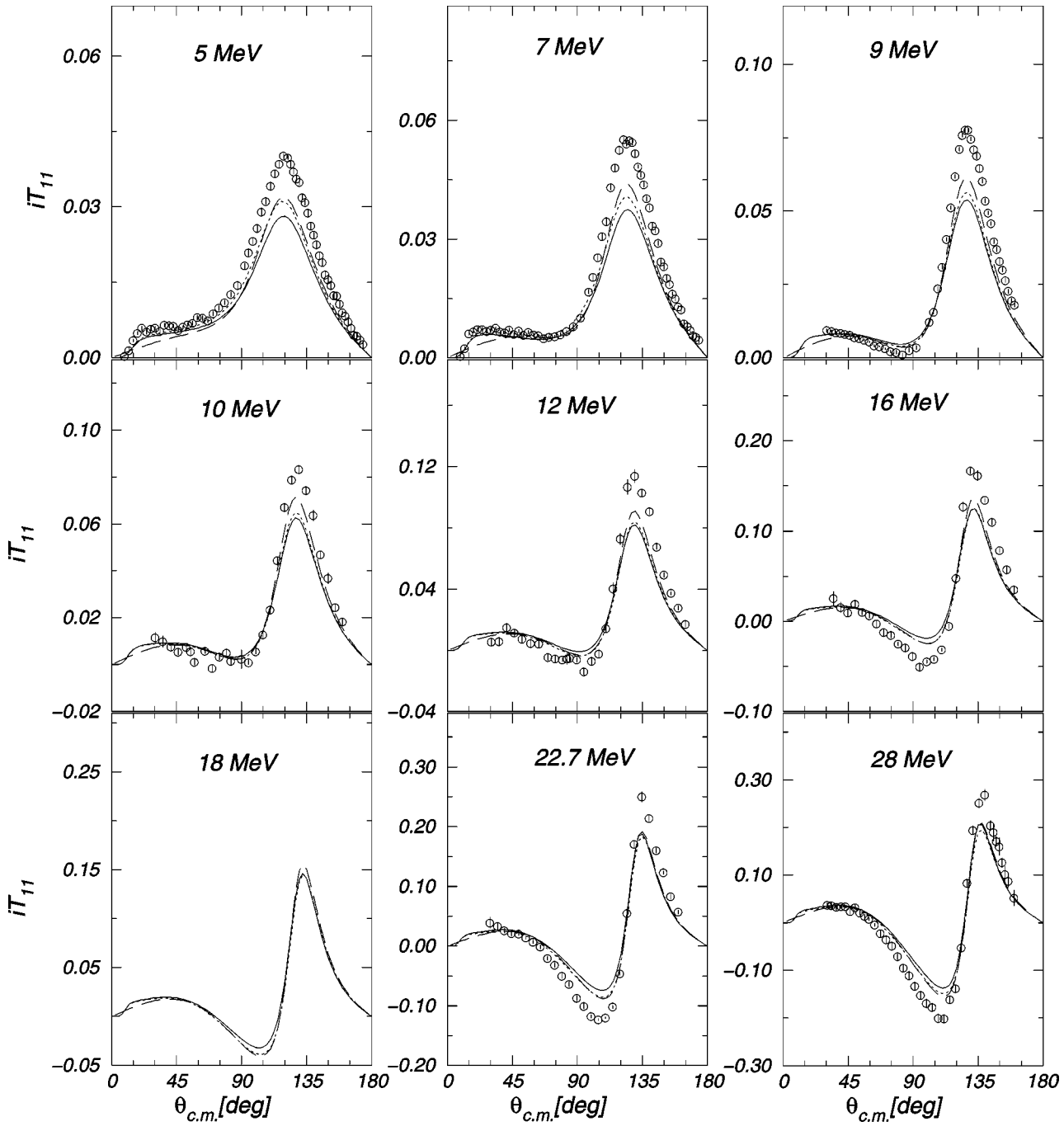

FIG. 5. Deuteron vector analyzing power iT_{11} up to 28 MeV. Calculations are shown for p-d scattering using the AV18 (solid line) and AV18+UR (dotted line) potentials and for n-d scattering using the AV18 potential (dashed line). Data are from Ref. [24] at $E_{\rm lab}=5,7,9$ MeV, from Ref. [25] at $E_{\rm lab}=10,12,16.5,22.7$ MeV, and from Ref. [22] at $E_{\rm lab}=28$ MeV.

better described with the AV18+UR potential. Conversely the description of the minimum of T_{20} and T_{21} is better described by the AV18 potential alone. The case of T_{21} is again of interest since 3NF effects seem to be bigger in this tensor observable than in the others. Unfortunately experimental data for T_{21} are not available at all the energies.

In order to give a quantitative estimation of the agreement between the theoretical calculations and the measurements, the χ^2_N for the polarization observables is presented in Table III. In the first row of the table, the χ^2_N is given with respect to a recent measurement performed at 1 MeV [43] and in the second row with respect to the measurements of Ref. [8] at $E_{\rm lab}=3$ MeV. These two energies are below the DBT and are useful for analyzing the trend of χ^2 starting at low energies. By inspection of the table, the manifestation of the A_y puzzle is evident since the χ^2_N for the vector observables is a few hundreds at low energy. Above 18 MeV A_y and iT_{11} change shape being closer to the shape of T_{21} with a pronounced minimum followed by a maximum. After that energy the values of χ^2_N decrease in such a way that, at the last

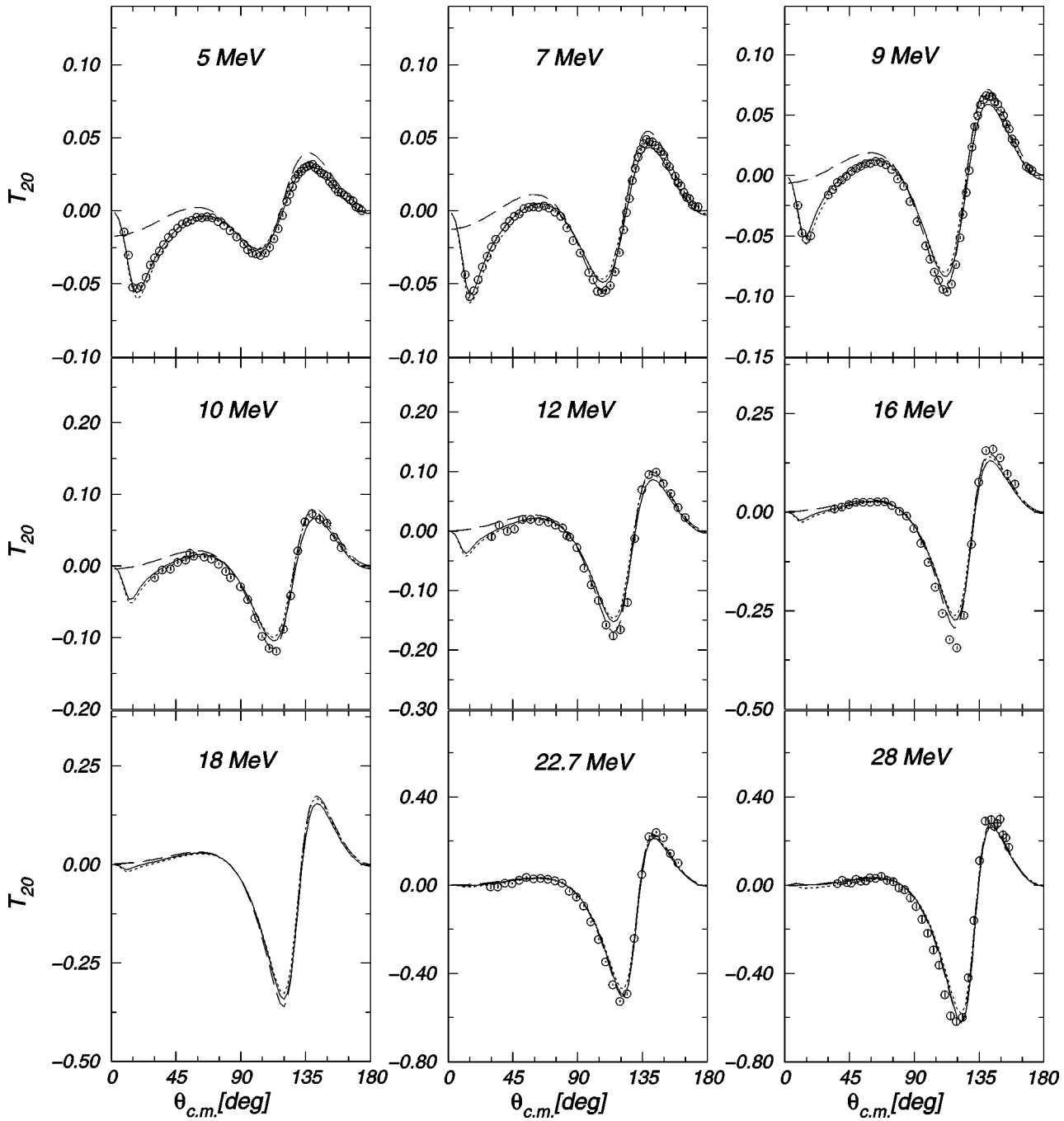

FIG. 6. Tensor analyzing power T_{20} up to 28 MeV. Calculations are shown for p-d scattering using the AV18 (solid line) and AV18 +UR (dotted line) potentials and for n-d scattering using the AV18 potential (dashed line). Data are from Ref. [24] at $E_{\rm lab}=5,7,9$ MeV, from Ref. [25] at $E_{\rm lab}=10,12,16.5,22.7$ MeV, and from Ref. [22] at $E_{\rm lab}=28$ MeV.

energy, vector and tensor observables have similar values which are of the order of one tenth. These final values are comparable to those ones obtained recently in Ref. [46] at 135 MeV.

VI. CONCLUSIONS

In the present paper we have studied p-d elastic scattering above the DBT, up to $E_{\rm lab}=28$ MeV. The differential cross section and the total breakup cross section as well as the vector and tensor analyzing powers have been calculated using one of the modern NN interactions, namely, the AV18 potential. In order to evaluate 3NF effects the three-nucleon potential of Urbana has been taken into account. The effects of the Coulomb interaction has been considered in the framework of the complex Kohn variational principle.

The internal part of the p-d scattering wave function has been expanded in terms of the PHH basis. The KVP has been applied to obtain a set of differential equations for the hyperradial functions. The set has been solved imposing outgoing

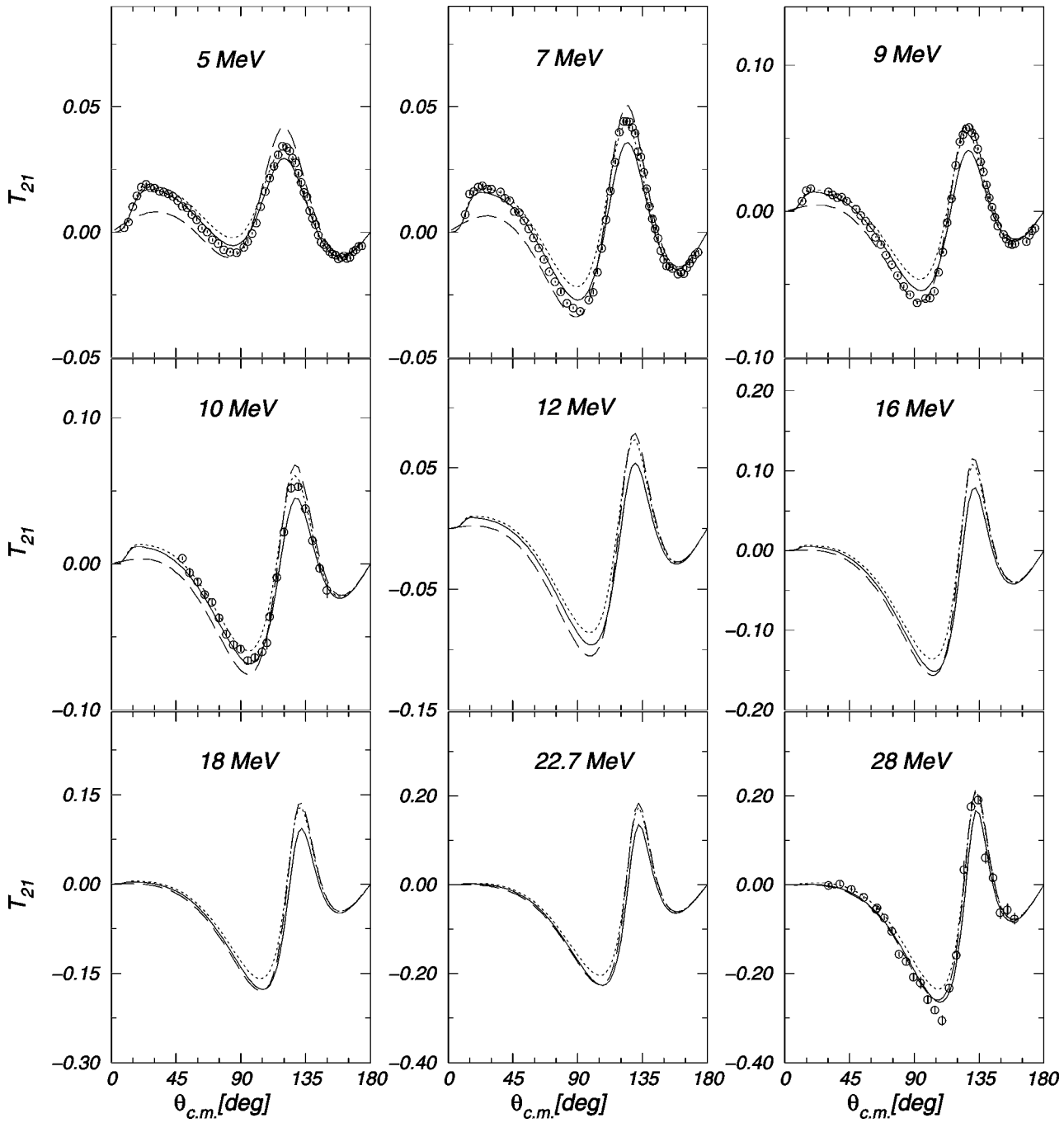

FIG. 7. Tensor analyzing power T_{21} up to 28 MeV. Calculations are shown for p-d scattering using the AV18 (solid line) and AV18 + UR (dotted line) potentials and for n-d scattering using the AV18 potential (dashed line). Data are from Ref. [24] at $E_{\rm lab}=5,7,9$ MeV, from Ref. [25] at $E_{\rm lab}=10$ MeV, and from Ref. [22] at $E_{\rm lab}=28$ MeV.

boundary conditions at a certain value of the hyperradius $\rho = \rho_0$ and expanding the hyperradial functions in the region $[0,\rho_0]$ in Laguerre polynomials plus an auxiliary oscillating function. The solution should not depend on the value of ρ_0 providing that for $\rho > \rho_0$ the asymptotic behavior has been reached. Such a technique has proved to be adequate since the results from Ref. [31] has been reproduced as well as the benchmark of Ref. [37].

The calculations have been extended to all states and parities with $J \leqslant 19/2$, corresponding to nine energies up to $E_{\rm lab} = 28$ MeV. The elastic S matrix has then been used to calculate the observables of interest and compare them to the data. Moreover, the corresponding observables for n-d scattering, where the Coulomb interaction is absent, have been calculated too. From the analysis of the results some conclusions can be drawn about the capability of the AV18 and AV18+URIX interactions to reproduce the data. A quantitative measure of the agreement achieved by the theory in the

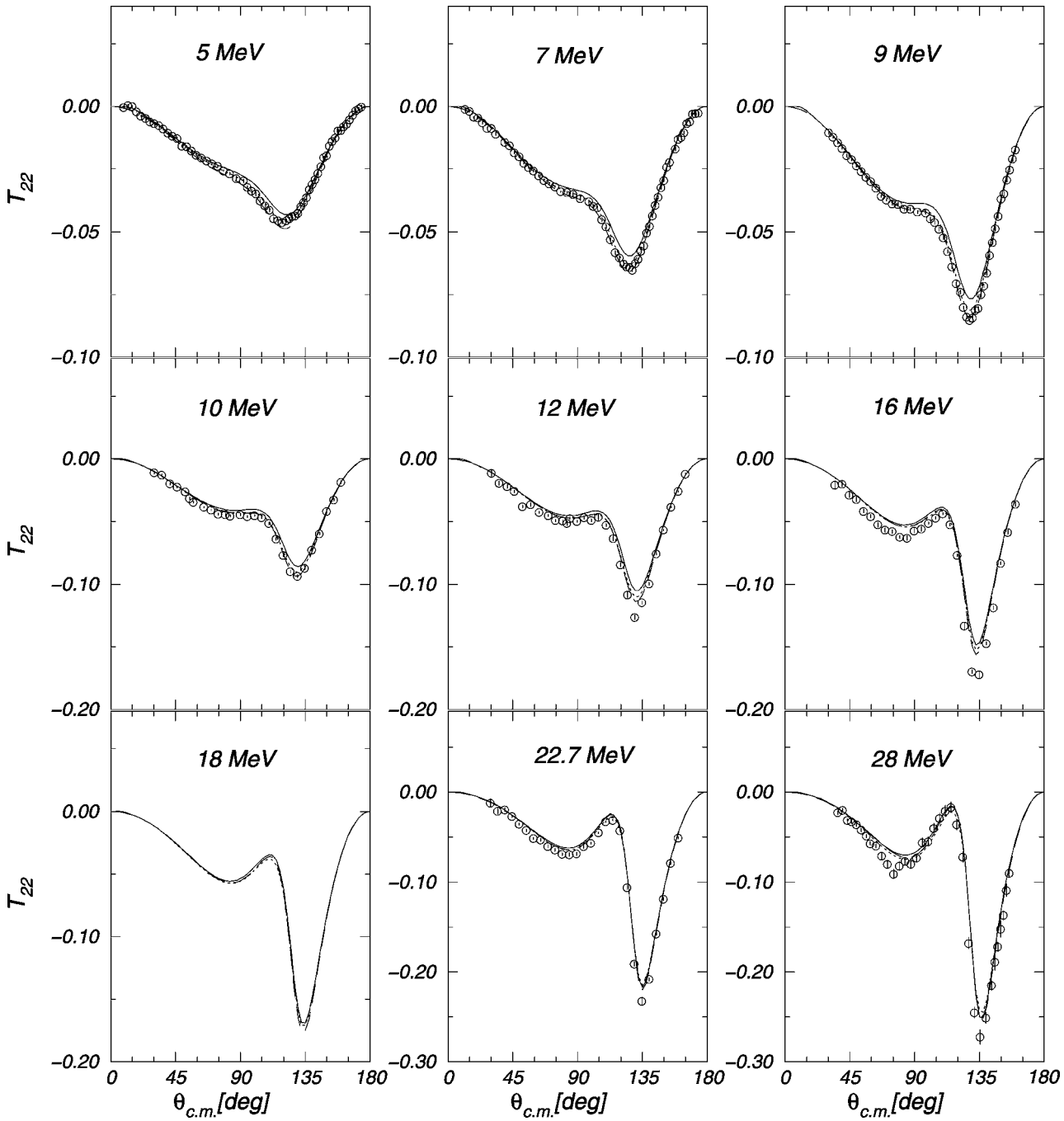

FIG. 8. Tensor analyzing power T_{22} up to 28 MeV. Calculations are shown for p-d scattering using the AV18 (solid line) and AV18 + UR (dotted line) potentials and for n-d scattering using the AV18 potential (dashed line). Data are from Ref. [24] at $E_{\rm lab}=5,7,9$ MeV, from Ref. [25] at $E_{\rm lab}=10,12,16.5,22.7$ MeV, and from Ref. [22] at $E_{\rm lab}=28$ MeV.

description of the data has been given through a χ^2 analysis. No appreciable 3NF effects have been observed in the total breakup cross section and small effects appear in the differential cross section. However, results using the AV18 + URIX model produce a lower χ^2_N value than those where the AV18 interaction has been used alone. At low energies this is a manifestation of the correct description of the ^{3}He binding energy by the AV18+URIX interaction. But as the energy increases, there is a different sensitivity to the 3NF. In particular, at the highest energy considered, $E_{\rm lab}=28$ MeV, the AV18+URIX differential cross section is above the AV18 differential cross section, reversing the order observed at lower energies. This situation becomes much more evident, for example, at $E_{\rm lab}=60$ MeV [4]. In order to further analyze this behavior in Table II the minimum of the AV18 and AV18+URIX cross sections are compared to the data. The minimum of the n-d differential cross section calculated with the AV18 potential is also given in order to estimate Coulomb effects. The results of the table are useful for analyzing what has been called the ''Sagara discrepancy'' [51].

In the case of vector and tensor analyzing powers the Urbana 3NF has little impact below 30 MeV. The centrifugal barrier is still strong and there is not too much sensitivity to the short range part of the interaction. Conversely there are important Coulomb effects. In order to improve the description of the vector analyzing powers new terms could be considered in the three-nucleon potential. In such a case both the vector and the tensor analyzing powers should improve as well.

The present picture of the $3N$ scattering from the theoretical point of view is the following. At low energies there is a large underprediction of the vector analyzing powers whereas the differential cross section and tensor analyzing powers are well described. Up to 30 MeV we see an improvement in A_y and iT_{11} indicating that the A_y puzzle is a low-energy problem. On the other hand, a progressive deterioration in the description of the cross section and tensor observables is revealed through a χ^2 analysis. For energies above 30 MeV we can refer to the very recent work of Ref. [4] and we see that this picture remains essentially the same up to very high energies (around 135 MeV). Above this energy a number of new conflicts appears.

At present a few realistic local and nonlocal NN interactions have been determined by accurately fitting the two nucleon scattering observables. All of them give rise to the A_y puzzle in the three-nucleon system. It seems difficult to derive a new NN interaction, which still accurately fits the two-nucleon scattering, and correctly describes the N-d A_y at low energies [52]. So, if this is the case, a possible solution to the puzzle should come from an improvement of the currently used 3NF models. Indeed, in accordance with chiral perturbation theory, these 3NF's include those terms of larger magnitude. On the other hand, the A_y puzzle can be solved by rather small changes in certain P-wave phase shifts, which can be obtained by adding a small term to the three-nucleon potential [47]. However, as the energy increases other discrepancies arise in the polarization observables that could have different origins. Hence, since the three-nucleon continuum can be calculated at present with great accuracy, it is reasonable to expect that the actual 3NF models can be adjusted to describe the $3N$ data. The necessary calculations will require large computing time, but is our opinion that this project will certainly help to understand the long unsolved problems in low-energy nuclear physics.

ACKNOWLEDGMENTS

One of us (A.K.) would like to thank W. Tornow, E. Ludwig, H. Karwowski, and C. Brune for useful discussions, and the Triangle Universities Nuclear Laboratory for hospitality and support where part of this work was performed. The authors wish to thank L. Lovitch for a critical reading of the manuscript.

[1] A. Kievsky, S. Rosati, and M. Viviani, Phys. Rev. Lett. **82**, 3759 (1999).
[2] M. Viviani, A. Kievsky, and S. Rosati, Few-Body Syst. **30**, 39 (2001).
[3] W. Glöckle *et al.*, Phys. Rep. **274**, 107 (1996).
[4] H. Witala *et al.*, Phys. Rev. C **63**, 024007 (2001).
[5] T. N. Rescigno, M. Baertschy, W. A. Isaacs, and C. W. McCurdy, Nature (London) **286**, 2474 (1999).
[6] E. O. Alt, W. Sandhas, and H. Ziegelmann, Phys. Rev. C **17**, 1981 (1978); E. O. Alt and W. Sandhas, *ibid.* **21**, 1733 (1980); E. O. Alt, A. M. Mukhamedzhanov, and A. I. Sattarov, Phys. Rev. Lett. **81**, 4820 (1998).
[7] A. Kievsky, J. Payne, J. Friar, S. Rosati, and M. Viviani, Phys. Rev. C **63**, 064004 (2001).
[8] S. Shimizu *et al.*, Phys. Rev. C **52**, 1193 (1995).
[9] L. D. Knutson, L. O. Lamm, and J. E. MacAninch, Phys. Rev. Lett. **71**, 3762 (1993).
[10] C. R. Brune *et al.*, Phys. Lett. B **428**, 13 (1998).
[11] A. Kievsky, S. Rosati, W. Tornow, and M. Viviani, Nucl. Phys. **A607**, 402 (1996).
[12] H. Witała and W. Glöckle, Nucl. Phys. **A428**, 48 (1991); H. Witała, D. Hüber, and W. Glöckle, Phys. Rev. C **49**, R14 (1994).
[13] A. Kievsky, M. Viviani, and S. Rosati, Nucl. Phys. **A551**, 241 (1993).
[14] M. Viviani, A. Kievsky, and S. Rosati, Few-Body Syst. **18**, 25 (1995).
[15] A. Kievsky, M. Viviani, and S. Rosati, Nucl. Phys. **A577**, 511 (1994).
[16] A. Kievsky, M. Viviani, and S. Rosati, Phys. Rev. C **52**, R15 (1995).
[17] M. Viviani, S. Rosati, and A. Kievsky, Phys. Rev. Lett. **81**, 1580 (1998).
[18] M. Viviani, A. Kievsky, L. E. Marcucci, S. Rosati, and R. Schiavilla, Phys. Rev. C **61**, 064001 (2000).
[19] L. E. Marcucci, R. Schiavilla, M. Viviani, A. Kievsky, and S. Rosati, Phys. Rev. Lett. **84**, 5959 (2000).
[20] R. B. Wiringa, V. G. J. Stoks, and R. Schiavilla, Phys. Rev. C **51**, 38 (1995).
[21] B. S. Pudliner *et al.*, Phys. Rev. Lett. **74**, 4396 (1995).
[22] K. Hatanaka *et al.*, Nucl. Phys. **A426**, 77 (1984).
[23] J. Sowinski, D. D. Pun Casavant, and L. Knutson, Nucl. Phys. **A464**, 223 (1987).
[24] K. Sagara *et al.*, Phys. Rev. C **50**, 576 (1994); K. Sagara (private communication).
[25] W. Grüebler *et al.*, Nucl. Phys. **A398**, 445 (1983); F. Sperisen *et al.*, *ibid.* **A422**, 81 (1984).
[26] J. Nuttall, Phys. Rev. Lett. **19**, 473 (1967); F. A. McDonald and J. Nuttall, *ibid.* **23**, 361 (1969); G. Doolen and J. Nuttall, J. Math. Phys. **12**, 2198 (1971).
[27] S. P. Merkuriev, Nucl. Phys. **A233**, 395 (1974).
[28] L. Rosenberg, Phys. Rev. D **8**, 1833 (1973).
[29] R. R. Lucchese, Phys. Rev. A **40**, 6879 (1989).
[30] A. Kievsky, Nucl. Phys. **A624**, 125 (1997).
[31] A. Kievsky, M. Viviani, and S. Rosati, Phys. Rev. C **56**, 2987 (1997).
[32] A. Kievsky, L. Marcucci, S. Rosati, and M. Viviani, Few-Body Syst. **22**, 1 (1997).

[33] S. P. Merkuriev, Ann. Phys. (N.Y.) **130**, 395 (1980); Yu. A. Kuperin, S. P. Merkuriev, and A. A. Kvitsinskii, Sov. J. Nucl. Phys. **37**, 857 (1983).
[34] E. O. Alt and A. M. Mukhamedzhanov, Phys. Rev. A **47**, 2004 (1993).
[35] J. L. Friar and G. L. Payne, in *Coulomb Interactions in Nuclear and Atomic Few-Body Collisions*, edited by F. S. Levin and D. Micha (Plenum, New York, 1996), p. 97.
[36] A. Kievsky, C. R. Brune, and M. Viviani, Phys. Lett. B **480**, 250 (2000).
[37] J. L. Friar *et al.*, Phys. Rev. C **51**, 2356 (1995).
[38] D. Hüber, J. Golak, H. Witała, W. Glöckle, and H. Kamada, Few-Body Syst. **19**, 175 (1995).
[39] R. G. Seyler, Nucl. Phys. **A124**, 253 (1969).
[40] J. H. Gibbons and R. L. Macklin, Phys. Rev. **114**, 571 (1959).
[41] R. F. Carlson *et al.*, Lett. Nuovo Cimento Soc. Ital. Fis. **8**, 319 (1973).
[42] T. C. Black, Ph.D. thesis, University of North Carolina at Chapel Hill, 1995, available from University Microfilms, Ann Arbor, MI 48106.
[43] M. H. Wood *et al.* (in preparation).
[44] A. Kievsky *et al.*, Phys. Rev. C **63**, 024005 (2001).
[45] C. Brune *et al.*, Phys. Rev. C **63**, 044013 (2001).
[46] H. Sakai *et al.*, Phys. Rev. Lett. **84**, 5288 (2000).
[47] A. Kievsky, Phys. Rev. C **60**, 034001 (1999).
[48] L. Canton and W. Schadow, Phys. Rev. C **63**, 034004 (2001).
[49] E. Epelbaum *et al.*, nucl-th/0007057.
[50] M. Viviani *et al.*, Phys. Rev. Lett. **86**, 3739 (2001).
[51] Y. Koike and S. Ishikawa, Nucl. Phys. **A631**, 683c (1998).
[52] D. Hüber and J. L. Friar, Phys. Rev. C **58**, 674 (1998).